Interferon-Beta Inhibits Human Glioma Stem Cells Rather Than Neural Stem Cells via Cell Cycle and Immune Signaling

Xin-Xin Han (xxhan@fudan.edu.cn)
Fudan University

Shengkai Jin
Tongji University

Li-Ming Yu
Fudan University

Min Wang
Jiaxing University

Xinyu Hu
Tongji University

Daiyu Hu
Tongji University

Jie Ren
Tongji University

Meng-Han Zhang
Fudan University

Wei Huang
Fudan University

Jia-Jia Deng
Fudan University

Qing-Qing Chen
Fudan University

Zhengliang Gao
Tongji University

Hua He
Second Military Medical University

Chunhui Cai
Tongji University

Research

Keywords: Glioma stem cells, IFN-β, neural stem cell, cell cycle, immune response

Posted Date: February 25th, 2021

DOI: https://doi.org/10.21203/rs.3.rs-241239/v1

Interferon-beta inhibits human glioma stem cells rather than neural stem cells via cell cycle and immune signaling

Xin-Xin Han[1]†*, Shengkai Jin[2]†, Li-Ming Yu[1], Min Wang[4], Xin-Yu Hu[3], Dai-Yu Hu[3], Jie Ren[3], Meng-Han Zhang[1], Wei Huang[1], Jia-Jia Deng[1], Qing-Qing Chen, Zhengliang Gao[3], Hua He[5,6]*, Chunhui Cai[3]*

[1] Shanghai Key Laboratory of Craniomaxillofacial Development and Diseases, Shanghai Stomatological Hospital, Fudan University, Shanghai, China.
[2] Institute of Photomedicine, Shanghai Skin Disease Hospital, Tongji University School of Medicine,Shanghai, China.
[3] Tongji University Cancer Center, Shanghai Tenth People's Hospital, School of Medicine, Tongji University, Shanghai, China.
[4] School of Medicine, Jiaxing University, Jiaxing, China.
[5] Department of Neurosurgery, Changzheng Hospital, Second Military Medical University, Shanghai, China.
[6] Department of Neurosurgery, Third Affiliated Hospital of Second Military Medical University, Shanghai, China.

*** Correspondence:**
Xin-Xin Han
xxhan@fudan.edu.cn

Hua He
hehua1624@smmu.edu.cn

Chunhui Cai
pattycaich@tongji.edu.cn

†These authors have contributed equally to this work

Abstract

Background: Malignant Glioma is considered to be a highly heterogeneous brain tumor, which may have originated from mutated neural stem cells (NSCs) many years before it was diagnosed. Malignant Glioma is characterized by strong self-renewal potential and immature differentiation potential. The main reason is that malignant glioma holds a key cluster cells, glioma stem cells (GSCs). GSCs contribute to tumorigenesis, tumor progression, recurrence, and treatment resistance. Interferon-beta (IFN-β) is well known for its anti-proliferative efficacy in diversity cancers. IFN-β also displayed potent antitumor results in malignant glioma. IFN-β treatments administered in response to gliomas affect both GSCs and NSCs. However, the function comparison, similarities and differences of IFN-β on GSCs and NSCs are rarely reported.
Methods: We used human GSCs and NSCs to detect the response difference between two cells by IFN-β. Human GSCs were constructed by ourselves and human normal NSCs line were differentiated from human embryonic stem cells. Various concentrations of IFN-β were separately used to treat human GSCs (hGSCs) and human NSCs (hNSCs). Cell morphology, growth, expression of special stemness genes, neural-related makers or proliferation related genes were staining and observed, such as SRY-box transcription factor 2 (Sox2), S100 calcium binding protein B (S100-beta) and marker of proliferation Ki-67 (Ki67). Genes alterations were carefully analyzed by RNA-seq. We used

repetitive stimulation treatment and compared the different response between hGSCs and hNSCs with IFN-β. Transcriptome analysis was also performed to identify genes with changes in expression levels in hGSCs but stable expression levels in hNSCs.
Results: We found that IFN-β preferentially inhibited GSCs rather than NSCs. The cell body and nucleus size of GSCs increased after IFN-β treatment. The expression of special stemness gene Sox2 and marker of proliferation Ki67 significantly decreased. S100-beta, which was a central nervous system enrichment, cycle progression and differentiation related gene, also reduced after IFN-β treatment. Significant differences were observed between hGSCs and human NSCs after continuous IFN-β treatment. Transcriptome analysis revealed the enrichment of the immune response, cell adhesion, cell cycle, and ribosome pathways such as proto-oncogene NF-kB subunit (*RELB*), TRAF interacting protein with forkhead associated domain (*TIFA*), nuclear factor kappa B subunit 1 (*NFKB*)and signal transducer and activator of transcription 6 (*STAT6*). Several typical cyclin genes, including cyclin A2 (*CCNA2)*, cyclin B1 (*CCNB1)*, cyclin B2 (*CCNB2),* and cyclin D1 (*CCND1)*, were significantly downregulated in GSCs after IFN-β stimulation.
Conclusions: Our study revealed how genetic diversity resulted in differential effects in response to IFN-β treatment. These results may contribute to improve the applications of IFN-β anti-cancer immunotherapy. In addition, these results may also help to design more effective pharmacological strategies to target killing cancer stem cells while protecting normal neural stem cells.

Keywords: Glioma stem cells, IFN-β, neural stem cell, cell cycle, immune response

Introduction

Malignant glioma is highly aggressive and represents the most common primary brain tumors. The overall survival period is typically less than 15 months. Even with regular therapy, including surgical resection and chemoradiation, tumor recurrence appears to be inevitable [1]. Approximately 70% of malignant glioma patients experience disease progression within one year of diagnosis [2]. Thus, the use of personalized drugs that target molecular receptors and immunotherapy have been viewed as promising new options for glioma treatment [3].

Malignant glioma is heterogeneous, with multiple epigenetic and genetic variations identified in associated tumor cells. The intrinsic, aggressive behavior of malignant glioma has also been shown to depend on the complex tumor microenvironment (TME). Malignant glioma and their TME consist of GSCs, mature neural cells (oligodendrocytes, astrocytes, microglia, and ependymal cells), and some immune cells etc [4,5].

The identification of cancer stem cells in malignant glioma are first reported in 2002 [6]. Several groups isolate and characterize stem-like cancer cells in glioma [6-8], which lead to the realization that GSCs are resistant to chemotherapy and radiotherapy [9,10]. Some groups try to find the genes which regulate GSCs maintenance and glioma progression [11-17]. Inspite of so many struggles, the prognosis of GBM has not enhanced in the past decade [17]. At the same time, the underlying mechanisms of GSCs survival after treatment remain unclear.

Interferon (IFN) factors are pleiotropic cytokines that can be categorized into 3 classes. Type I IFNs include approximately 20 members. Human IFNs induce the Janus kinase–signal transducer (JAK) and activator of transcription (STAT) cascade by binding to the IFN-α/β receptors (IFNARs), IFNAR1 and IFNAR2 [18,19]. IFN-β signaling is needed for its antiproliferative effects on a variety of cancer cells [20-24]. During malignant glioma treatment, at least two aspects of NSCs are related to GSCs. On the one hand, mutated NSCs are considered to be the initiation cells of glioma [17,25,26]. On the other hand, normal NSCs are considered to have the ability to move towards

GSCs, and can be used as carriers for the treatment of gliomas [27,28]. The human F3 NSCs cell line has been used in multiple studies to perform NSC-based gene therapy, delivering both IFN-β and cytosine deaminase (CD)/5-fluorocytosine (5-FC) prodrugs to glioma cells [29-31]. Although IFN-β has been generally employed as a clinical treatment, whole-transcriptome analyses examining the effects of IFN-β stimulation in GSCs and NSCs are still rare. A systematic understanding of the genetic variations that occur following IFN-β treatments can provide additional evidence for the optimization of IFN-β-associated gene therapy for malignant glioma treatment in clinical trials.

In the present study, we used various concentrations of IFN-β to separately treat human GSCs (hGSCs) and human NSCs (hNSCs). Both morphological and genetic alterations were carefully observed and analyzed. We found that IFN-β decreased the cell and nuclear sizes of hGSCs. The number of sphere-like cells observed in hGSC populations was reduced, both during short-term treatments and under conditions of continuous stimulation. However, INF-β did not appear to have the same or similar effects on hNSCs. Transcriptome analysis was performed to identify genes with changes in expression levels in hGSCs but stable expression levels in hNSCs. Immune response and cell adhesion genes were upregulated by IFN-β treatment, whereas the expression levels of cell cycle and ribosome genes were strongly reduced, which was consistent with our observations of the cellular morphology. We observed that IFN-β preferentially restrained hGSCs rather than hNSCs. A few cyclin genes *CCNA2*, *CCNB1/2* and *CCND1*, reduced in hGSCs after IFN-β treatment. Our exploration may facilitate to design new and more effective pharmacological strategies for killing hGSCs while protecting hNSCs during glioma treatment.

Materials and methods

Cell culture

hGSCs line was established from surgical specimens. Surgical specimens were gotten strictly according to Ethics Committee permission. Patients with glioma provided informed consent and donated surgical specimens sample to the study. All the tumor samples were taken to the laboratory in time for continuation dealing. Briefly, after surgery, surgical specimens were collected for primary culture. The specimens were washed with 1× Hank's Balanced Salt Solution (HBSS, Gibco) at least six times. Then, the specimens were cut into small pieces, and the tissue fragments were placed into centrifuge tubes containing 1 U/mL Dispase II (Roche) in 3 mL Dulbecco's Modified Eagle Medium (DMEM)/F12 (Gibco) and kept in water-bath at 37°C for 30 minutes to allow digestion. After digestion, the specimens were centrifuged at 1,000 × g for 3 minutes. The supernatant was discarded, and the tissues were resuspended with 3 mL DMEM/F12, followed by centrifugation. Finally, the precipitate was resuspended in growth medium (DMEM/F12 supplemented with N-2, B-27, GlutaMAX, bFGF, EGF, heparin and penicillin-streptomycin) for daily culture. All the work concentration of FGF, EGF and heparin were 20 ng/Ml, N-2, GlutaMax and penicillin-streptomycin were 100X while B-27 were 50X in the culture medium.

hNSCs line was generated from human embryonic stem cells (hESCs) [32]. Brief description, StemPro Accutase (Thermo Fisher) was used to digest the hESCs for 20 min at 37°C. The cells were plated onto gelatin-coated plates for 1 hour at 37°C. Because hESCs remain suspended, whereas mouse embryonic fibroblast (MEF) cells are adherent and separate hESCs from MEFs. The non-adherent hESCs were washed and seeded on Matrigel-precoated dishes in MEF-conditioned medium. Then we changed the medium to remove the ROCK inhibitor after 24 hours. Single adherent hESCs were expanded in cell medium until they were almost confluent. Noggin (500 ng/mL, R&D) and transforming growth factor-beta (TGF-β) inhibitor (10 mmol/L, Tocris) were added to confluent cells.

The medium was replaced every 2 days with fresh KSR medium and different concentration gradients N2B27 medium. After nearly 10 days of differentiation, NSCs were cultured with 100% N2 medium (DMEM/F12 supplemented with N2, B27, GlutaMAX, FGF, EGF, heparin, penicillin, and streptomycin) for 1 day and then transferred into a 100% N2/B27 medium (DMEM/F12 supplemented with N2, B27,GlutaMAX, FGF, EGF, heparin, penicillin and streptomycin).

Plate coating

Plates were coated with gelatin (Sigma) or Matrigel (BD) for NSCs induction. Culture plates were precoated with poly-L-ornithine (Sigma) and laminin (Thermo Fisher) for human NSCs cultures. The 24-well plates and 6-well plates were freshly coated with gelatin or Matrigel and incubated overnight at 4°C for better packing effects. The next day, the dishes were treated with 0.5 μg/mL poly-L-ornithine (dissolved in water) at room temperature for 16 hours. Then, we washed the dishes with 1× phosphate-buffered saline (PBS). Finally, 5 μg/mL laminin was added to the dishes for at least 16 hours. The coated dishes were stored at −20°C, and the supernatant was discarded before use.

Cell immunofluorescent staining

hGSCs were assessed using a staining assay, similar to that described in our previous study [32]. In brief, hGSCs were grown for 3 or 7 days in optimized culture conditions and fixed in 4% paraformaldehyde (PFA) for 12 minutes. Then, the cells were permeabilized using 2.5% Triton X-100 in PBS and incubated for 15 minutes. We discarded the supernatant and blocked all non-specific reactions with 5% bovine serum albumin (Solarbio) in 1× PBS for 1.5 hours. All procedures were performed at room temperature. hGSCs were incubated in primary antibodies against Sox2 (Goat, R&D), S100-β (Mouse, Abcam), or Ki67 (Rabbit, Thermo Fisher) for 2 days at 4°C. After three washes with 0.1% Tween-20 (Sigma) in 1× PBS, the cells were exposed to secondary antibodies (Jackson Immuno Research), including Alexa Fluor 633-conjugated donkey anti-goat IgG antibody, Alexa Fluor 488-conjugated donkey anti-mouse IgG antibody, Alexa Fluor Cy3-conjugated donkey anti-goat IgG antibody, and Alexa Fluor 633-conjugated donkey anti-rabbit antibody. The antibodies were dissolved in PBS containing 2.5% bovine serum albumin and incubated with the cells at room temperature for 2 hours. Finally, the cells were washed 3 times with 0.1% Tween-20 in PBS, and 4', 6-diamidino-2-phenylindole (DAPI, Sigma) was used to stain the nuclei. An inverted fluorescence microscope (Nikon TE2000) was used to obtain images of the immunofluorescent-stained cells.

Sequencing and transcriptome analysis

We collected both hGSCs and hNSCs after 7 days of culture. After discarding the supernatant medium, 1× PBS was used to wash the cells once, and 2 ml Trizol (Invitrogen, Carlsbad, CA, USA) was added to each plate for RNA extraction. The RNA integrity was determined using an Agilent 2100 Bioanalyzer (Agilent, Palo Alto, CA, USA). The quantity was determined on a Nanodrop (Thermo Fisher Scientific, Wilmington, DE, USA). Poly-A containing mRNA molecules were purified by using ploy-T oligo-attached magnetic beads, followed by fragmentation and priming for cDNA synthesis using an Illumina TruSeqTM RNA sample preparation kit (Illumina Inc., San Diego, CA, USA), according to the manufacturer protocol. The cDNA was further converted into double-

stranded DNA using the reagents supplied in the kit. The dsDNA was purified with AMpure XP beads and was then end-repaired and A-tailed, according to Illumina's protocol. After adapter ligation, PCR was applied to enrich the DNA fragments with adapter molecules on both ends and to amplify the amount of DNA in the library. The resulting molecular libraries were pooled together and sequenced on a HiSeq 2500 sequencer (Illumina Inc.). Then, the fragments per kilobase of transcript per million mapped reads (FPKM) values were analyzed as the gene expression base. Differentially expressed gene (DEG) analysis was performed using online software (Morpheus, https://software.broadinstitute.org/morpheus) to identify up- and downregulated genes. Kyoto Encyclopedia of Genes and Genomes (KEGG) and Gene Ontology (GO) analyses were also performed using an online database (g:Profiler) [33].

Statistical Analysis

All data were collected and analyzed based on three or more replicates. The error bars represent the standard deviation of the mean. Statistical analysis was performed using GraphPad Prism version 8.0.0 for Windows, GraphPad Software, San Diego, California USA, www.graphpad.comGraphPad Prism 7.0. For multiple comparisons, Student's t-test was used to determine significant differences. Significance is indicated as *$p < 0.05$. **$p < 0.01$, and ***$p < 0.001$.

Results

IFN-β inhibits the growth of hGSCs

To detect the functional role of IFN-β in hGSCs, we firstly used IFN-β, at concentrations of 0, 0.625, 1.25, 2.5, 5, and 11 ng/mL, to treat the hGSCs (Fig. 1a). hGSCs typically display two types of cell morphologies: sphere-like hGSCs and adherent hGSCs (Fig. 1b). We quantified the sizes of the sphere-like hGSC and the coverage of adherent hGSCs to examine the effects of IFN-β on cell growth. The sizes of the sphere-like cells significantly decreased, even when using the lowest treatment dose of 0.625 ng/mL IFN-β (Fig. 1c). However, no changes in the coverage of adherent cells were observed until the treatment concentration reached 5 ng/mL IFN-β (Fig. 1d). These observations suggested that adherent hGSCs have a higher tolerance against IFN-β treatment than sphere-like cells. We repeated the treatment assay using higher IFN-β concentrations, including 11, 33, and 100 ng/mL, using both hGSCs and hNSCs (Fig. 1e, h). High concentrations of IFN-β also inhibited hGSC growth, but no significant morphological changes were observed among the treated hNSCs (Fig. 1f, i). The quantitative analysis of cell coverage supported our visual observations (Fig. 1g, j). In conclusion, both low-dose (0.625 ng/mL) and high-dose (up to 33 ng/mL) IFN-β treatments were able to block cell growth in hGSCs, without affecting hNSCs.

The nuclear sizes of hGSCs was decreased by IFN-β

We next performed immunostaining to detect the expression of Ki67, S100-β, and Sox2 in hGSCs after 6 days of treatment of IFN-β at both low (11 ng/mL) and high (33 ng/mL) doses. Similar to our morphological observations, the number of Ki67-positive hGSCs decreased after IFN-β treatment (Fig. 2a, b), as did the numbers of S100-β- and Sox2-positive cells (Fig. 2a, b). The quantitative

assessment of Ki67, S100-β, Sox2, and DAPI nuclear stain in hGSCs following IFN-β stimulation can be seen in Fig. 2c. Because the total cell number decreased, the ratio of Ki67 to DAPI staining did not show a difference between the control group and the IFN-β-treated group. Overlapping images showed that the relative expression level of S100-β increased significantly after IFN-β stimulation (Fig. 3a). IFN-β might represent an effective agent for controlling cell differentiation in hGSCs [34]. S100-β has long been considered a biomarker for astrocytes [35]. Recently, some studies have also identified the high expression levels of S100-β with malignant tumors [36]. The increased S100-β expression observed in hGSCs following IFN-β stimulation agrees with previous reports. The higher magnification image revealed the nuclear status (Fig. 3b). Representative images of DAPI staining and the schematic diagram of the nucleus revealed significant nuclear enlargement after IFN-β stimulation (Fig. 3c). The nucleus size was quantified using ImageJ, which revealed that the size of the nucleus increased in a dose-dependent manner following IFN-β treatment (Fig. 3d).

The cell growth and morphology of hGSCs was reduced by repetitive stimulation treatment with IFN-β

Clinically, IFN-β is administered over a long time course. Thus, we examined the effects of continuous IFN-β stimulation. Both hGSCs and hNSCs were cultured in either control medium or IFN-β medium for one generation (6 days), and then the control cells were passaged into control medium, whereas IFN-β-treated cells were separately passaged into both control medium and IFN-β medium (Fig. 4a), generating three groups of cells: control to control, IFN-β to control, and IFN-β to IFN-β. On day 2, the number of sphere-like hGSCs in the IFN-β to IFN-β group decreased compared with the numbers observed in the control to control group (Fig. 4b). The hGSCs conditions in IFN-β to control group showed more sphere-like cells than IFN-β to IFN-β group but fewer than observed in the control to control group. Although no significant effects were observed among hNSCs following short-term IFN-β stimulation (Fig. 1i), continuous IFN-β stimulation resulted in decreased cell growth (Fig. 4c). We observed these groups of cells again on day 8, which revealed very few surviving sphere-like cells in hGSCs within the IFN-β to IFN-β group (Fig. 4d). The enlargement of both the cell body and the nuclear size was also observed in this group (Fig. 4e). The hGSCs in the IFN-β to IFN-β group displayed an oligodendrocyte-like morphology, with a long and massive synapse (Fig. 4e). Quantitative analysis of hGSCs, including the coverage rate (Fig. 4f) and the single clone area (Fig. 4g), was performed on the surviving clones, which revealed significant reductions associated with IFN-β treatment.

Different gene responses in hGSCs and hNSCs after IFN-β treatment

To better understand the molecular mechanism associated with the IFN-β treatment effects observed in hGSCs and hNSCs, we performed RNA sequencing on samples treated with or without IFN-β in both hGSCs and hNSCs. Gene clustering analysis indicated the high quality of our whole-transcriptome data (Fig. 5a). The analysis of DEGs was used to identify genes that were up- and downregulated following IFN-β stimulation, resulting in 1,707 and 1,338 genes designated as $hGSC^{+}$ and $hGSC^{-}$ genes, respectively, whereas 1,553 and 1,169 genes were respectively designated as $hNSC^{+}$ and $hNSC^{-}$ genes (Fig. 5b). The integrative analysis of these four groups resulted in the identification of 995 genes characterized as $hGSC^{-}hNSC^{NA}$ (genes only downregulated in hGSCs but with no change in hNSCs) and 969 genes characterized as $hGSC^{+}hNSC^{NA}$ (genes only upregulated in hGSCs but with no change in hNSCs) (Fig. 5c). We then performed GO and KEGG analyses on

these two groups to further explore the potential downstream mechanisms associated with the response to IFN-β. The GO biological process (BP) analysis revealed that $hGSC^{+}hNSC^{NA}$ genes were primarily enriched in cytokine-mediated signaling, immune response, response to external stimulus, and cell adhesion pathways (Fig. 5d). The KEGG analysis revealed that $hGSC^{-}hNSC^{NA}$ genes were enriched in the cell cycle and ribosome pathways (Fig. 5e). Our whole-transcriptome analysis results agreed with our previous morphological observations, supporting increased cell adherence and decreased cell growth. The expression patterns of the immune response and cell adhesion genes were displayed as heatmaps for both hGSCs and hNSCs (Fig. 5f). Consistently with known IFN-β downstream pathways, *JAK2*, *STAT6*, and *NFKB1*/2 were identified within the immune response pathways [19,37,38]. We also explored the detailed expression patterns of 22 genes in the cell cycle pathway (Fig. 5g). Typical cell cycle-related genes, such as *CCNA2*, *CCNB1*, *CCNB2,* and *CCND1,* were significantly downregulated following IFN-β stimulation in hGSCs but remained unchanged in hNSCs.

IFN-β decreased cell proliferation in hGSCs

IFN-β decreased hGSCs cell growth on both the morphological and genetic levels. Cell cycle-related genes were significantly downregulated after IFN-β stimulation (Fig. 5g and 6). The number of sphere-like cells also reduced significantly following IFN-β treatment, and both cell body and nuclear size increased. Simultaneously, genes associated with cell adhesion were upregulated in hGSCs, which supported the observed reductions in sphere-like cells and the enlargement of the cell nucleus. We also observed multiple synapses in hGSCs under conditions of continuous stimulation with IFN-β, and this morphological change may be associated with changes in gene expression in the immune response pathway.

Discussion

Our results indicated that IFN-β affected hGSCs rather than hNSCs. hNSCs are considered to be the most likely initiation cells of malignant glioma[17,25,26]. On the other hand, hNSCs have been considered efficient vehicles for the delivery of anti-cancer agents to tumor sites during therapeutic applications [39,40]. IFN-β has been found to exert antiproliferative effects in many cancer cell types [41,42]. IFN-β can decrease cell proliferation and progression through the inhibition of the cell cycle S-phase in glioma cell lines [43]. However, the underlying molecular mechanisms responsible for the subsequent differences observed following IFN-β treatment between cancer stem cells and normal NSCs remain unclear. Microarray-based gene expression profiling performed in three glioma cell lines and primary B-cells following IFN-β treatment was reported in 2014 [44,45]. Several novel IFN-β response genes were identified in primary B-cells, including *NEXN*, *HAPLN3*, *DDX60L,* and *IGFBP4* [45]. In this study, RNA sequencing was performed to reveal the molecular mechanisms associated with the response to IFN-β. We explored potential IFN-β response genes in glioma cells by performing DEG analysis between hGSCs and hNSCs. A total of 969 genes were identified as IFN-β-upregulated genes, whereas 995 genes were identified as IFN-β-downregulated genes in hGSCs compared with hNSCs. This large number of genes provides multiple opportunities to identify potential therapeutic targets that can be combined with IFN-β treatments for clinical applications.

A previous study indicated that IFN-β could induce spherogenicity in hGSCs [44]. In our study, we observed a significant reduction in sphere-like cells following IFN-β stimulation. The GO analysis results indicated enrichment in cell adhesion genes, providing strong support for a functional role for IFN-β in cancer stem cell morphology. *NEXN* encodes nexilin, which acts as a linker protein for the cytoskeleton and plays a functional role in focal adhesion junctions [46]. *NEXN* was previously identified as a novel IFN-β response gene in multiple sclerosis [45]. In the whole-transcriptome analysis following IFN-β treatment, *NEXN* was identified as a top gene in the enriched cell adhesion pathway in hGSCs after IFN-β treatment. Therefore, *NEXN* may also represent a novel IFN-β response gene in hGSCs.

The genes that were downregulated by IFN-β treatment were primarily enriched in cell cycle pathways, which also provides evidence to support the previously identified inhibitory role of IFN-β in cancer cells [41-43]. A total of 22 cell cycle-related genes were found to be downregulated in hGSCs, but no significant differences were observed in hNSCs. We suggested that these 22 genes may play irreplaceable roles in response to IFN-β treatment in hGSCs. Recently, one study attempted to combine IFN-β treatment together with a novel, effective, cyclin-dependent kinase (CDK) inhibitor (TG02), which is used clinically to treat GBM [47-49], resulting in synergistic functions in human glioma models [18]. In our data, *CDK1* was identified in the transcriptome analysis. Many other well-known cell cycle-related genes, such as the cyclin family genes (*CCNB1*, *CCND2*, *CCNB2,* and *CCNA2*), and MCM family genes (*MCM4*, *MCM5,* and *MCM6*), were also identified. These results may facilitate the development of more efficient therapeutic options by guiding the selection of useful anti-tumor drugs.

Conclusions

In summary, our study established the inhibition effects of IFN-β in hGSCs rather than in hNSCs. Additional morphological details were observed following IFN-β stimulation, such as larger cell bodies, increased nuclear size, fewer sphere-like cells, and more oligodendrocyte-like synapses. The subsequently transcriptome analysis using RNA sequencing was highly consistent with our morphological observations of hGSCs. The enrichment of genes involved in the cell cycle and cell adhesion pathways supported the observed reduction in cell growth reduction and the morphological changes associated with IFN-β treatment. In addition, our exploration of the genetic modification that occurs after IFN-β treatment in both hGSCs and hNSCs. This may benefit the design of new and more effective pharmacological strategies for GBM treatment.

Abbreviations

NSCs: neural stem cells; GSCs: glioma stem cells; IFN-β: Interferon-beta; hNSCs: human NSCs; hGSCs: human GSCs; CCNA2: cyclin A2; CCNB1: cyclin B1; CCNB2: cyclin B1; CCND1: cyclin D1; TME: tumor microenvironment; JAK: Janus kinase–signal transducer; HBSS: Hank's Balanced Salt Solution; DMEM: Dulbecco's Modified Eagle Medium; MEF: mouse embryonic fibroblast; TGF-β: Transforming growth factor-beta; PBS: phosphate-buffered saline; PFA: paraformaldehyde; FPKM: fragments per kilobase of transcript per million mapped reads; DEG: Differentially expressed gene; KEGG: Kyoto Encyclopedia of Genes and Genomes; GO: Gene Ontology; BP: biological process; CDK: cyclin-dependent kinase; CD: cytosine deaminase; 5-FC :5-fluorocytosine.

Author Contributions

CCH, HXX, and HH conceived and designed the research. HXX and JSK performed the sample collection, experiments, and data analysis. YLM, WM, HXY, HDY, and RJ assisted with the performance of cell-based experiments. ZMH, HW, and DJJ assisted with data analysis. CCH, HXX, and JSK wrote the manuscript. All authors have read and approved the final version of the manuscript.

Funding

This work was supported by funds from the National Natural Science Foundation of China [31600819 to CCH, 81901031 to HXX, 32070862 and 31571058 to GZL], the Shanghai Municipal Population and Family Planning Commission [20174Y0216 to CCH], , the Natural Science Foundation of Shanghai [19ZR1445400 to HXX], the National Key R&D Program of China [2019YFA0110300], and the Shanghai Easter Scholar [8101219003 to GZL].

Availability of data and materials

All data and materials are available upon request.

Ethics approval and consent to participate

Surgical specimens were gotten strictly according to Ethics Committee permission in Shanghai Tenth People's Hospital.

Consent for publication

Not applicable.

Competing interests

The authors have no conflicts of interest to disclose.

References

[1] Ostrom T, Gittleman H, Xu J, Kromer C, Wolinsky Y, Kruchko C, et al. CBTRUS Statistical Report: Primary Brain and Other Central Nervous System Tumors Diagnosed in the United States in 2009-2013. Neuro Oncol 2016;18: v1-v75.

[2] Stupp R, Mason W. P, van den Bent M. J, Weller M, Fisher B, Taphoorn M J, et al. Radiotherapy plus concomitant and adjuvant temozolomide for glioblastoma. N Engl J Med. 2005;352: 987-996.

[3] Davis, M. E. Glioblastoma: Overview of Disease and Treatment. Clin J Oncol Nurs. 2016; 20: S2-8.

[4] Abels E. R, Broekman M. L. D, Breakefield X. O & Maas S. L. N. Glioma EVs Contribute to Immune Privilege in the Brain. Trends Cancer. 2019; 5: 393-396.

[5] Broekman M. L, Maas S. L. N, Abels E. R, Mempel T. R, Krichevsky A. M, Breakefield X. O. Multidimensional communication in the microenvirons of glioblastoma. Nat Rev Neurol. 2018; 14: 482-495.

[6] Ignatova T. N, Kukekov V. G, Laywell E. D, Suslov O. N, Vrionis F. D, Steindler D. A. Human cortical glial tumors contain neural stem-like cells expressing astroglial and neuronal markers in vitro. Glia. 2002; 39: 193-206.

[7] Galli R, Binda E, Orfanelli U, Cipelletti B, Gritti A, De Vitis S, et al. Isolation and characterization of tumorigenic, stem-like neural precursors from human glioblastoma. Cancer Research. 2004; 64: 7011-7021.

[8] Hemmati H. D, Nakano I, Lazareff J. A, Masterman-Smith M, Geschwind D. H, Bronner-Fraser M, et al. Cancerous stem cells can arise from pediatric brain tumors. P Natl Acad Sci USA. 2003; 100: 15178-15183.

[9] Bao S, Wu Q, McLendon R. E, Hao Y, Shi Q, Hjelmeland A. B, et al. Glioma stem cells promote radioresistance by preferential activation of the DNA damage response. Nature. 2006; 444: 756-760.

[10] Chen J, Li Y, Yu T. S, McKay R. M, Burns D. K, Kernie S. G, et al. A restricted cell population propagates glioblastoma growth after chemotherapy. Nature. 2012; 488: 522-526.

[11] Herrmann A, Lahtz C, Song J, Aftabizadeh M, Cherryholmes GA, Xin H, et al. Integrin α6 signaling induces STAT3-TET3-mediated hydroxymethylation of genes critical for maintenance of glioma stem cells. Oncogene. 2020; 39: 2156-2169.

[12] Hu B, Wang Q, Wang YA, Hua S, Sauvé CG, Ong D, et al. Epigenetic Activation of WNT5A Drives Glioblastoma Stem Cell Differentiation and Invasive Growth. Cell. 2016; 167: 1281-1295.

[13] Huang H, Yu X, Han X, Hao J, Zhao J, Bebek G, et al. Piwil1 Regulates Glioma Stem Cell Maintenance and Glioblastoma Progression. Cell Rep. 2021; 34: 108522.

[14] Kim JY, Kim HJ, Jung CW, Choi BI, Lee DH, Park MJ. PARK7 maintains the stemness of glioblastoma stem cells by stabilizing epidermal growth factor receptor variant III. Oncogene. 2021; 40: 508-521.

[15] Taga T. & Tabu K. Glioma progression and recurrence involving maintenance and expansion strategies of glioma stem cells by organizing self-advantageous niche microenvironments. Inflamm Regen. 2020; 40: 33.

[16] Venkatesh HS, Johung TB, Caretti V, Noll A, Tang Y, Nagaraja S, et al. Neuronal Activity Promotes Glioma Growth through Neuroligin-3 Secretion. Cell. 2015; 161: 803-816.

[17] Wang X, Zhou R, Xiong Y, Zhou L, Yan X, Wang M, et al. Sequential fate-switches in stem-like cells drive the tumorigenic trajectory from human neural stem cells to malignant glioma. Cell Res. 2021.

[18] Lohmann B, Le Rhun E, Silginer M, Epskamp M, Weller M. Interferon-beta sensitizes human glioblastoma cells to the cyclin-dependent kinase inhibitor, TG02. Oncol Lett. 2020; 19: 2649-2656.

[19] Platanias L. C. Mechanisms of type-I- and type-II-interferon-mediated signalling. Nat Rev Immunol. 2005; 5: 375-386.

[20] Borden E C, Lindner D, Dreicer R, Hussein M, Peereboom D. Second-generation interferons for cancer: clinical targets. Semin Cancer Biol. 2000; 10: 125-144.

[21] Mizuno, M. & Yoshida, J. Effect of human interferon beta gene transfer upon human glioma, transplanted into nude mouse brain, involves induced natural killer cells. Cancer Immunol Immun. 1998; 47: 227-232.

[22] Natsume A, Mizuno M, Ryuke Y, Yoshida J. Antitumor effect and cellular immunity activation by murine interferon-beta gene transfer against intracerebral glioma in mouse. Gene Ther. 1999; 6: 1626-1633.

[23] Natsume A, Tsujimura K, Mizuno M, Takahashi T, Yoshida J. IFN-beta gene therapy induces systemic antitumor immunity against malignant glioma. J Neuro-Oncol. 2000; 47: 117-124.

[24] Yagi K, Hayashi Y, Ishida N, Ohbayashi M, Ohishi N, Mizuno M, et al. Interferon-Beta Endogenously Produced by Intratumoral Injection of Cationic Liposome-Encapsulated Gene - Cytocidal Effect on Glioma Transplanted into Nude-Mouse Brain. Biochem Mol Biol Int. 1994; 32: 167-171.

[25] Alcantara Llaguno S, Sun D, Pedraza AM, Vera E, Wang Z, Burns DK, et al. Cell-of-origin susceptibility to glioblastoma formation declines with neural lineage restriction. Nat Neurosci. 2019; 22: 545-555.

[26] Tian A, Kang B, Li B, Qiu B, Jiang W, Shao F, et al. Oncogenic State and Cell Identity Combinatorially Dictate the Susceptibility of Cells within Glioma Development Hierarchy to IGF1R Targeting. Adv Sci (Weinh). 2020; 7: 2001724.

[27] Kendall S. E, Najbauer J, Johnston H. F, Metz M. Z, Li S, Bowers M, et al. Neural stem cell targeting of glioma is dependent on phosphoinositide 3-kinase signaling. Stem Cells. 2008; 26: 1575-1586.

[28] Schmidt N. O, Przylecki W, Yang W, Ziu M, Teng Y, Kim S. U, et al. Brain tumor tropism of transplanted human neural stem cells is induced by vascular endothelial growth factor. Neoplasia. 2005; 7: 623-629.

[29] Dickson P. V, Hamner J. B, Burger R. A, Garcia E, Ouma A. A, Kim S. U, et al. Intravascular administration of tumor tropic neural progenitor cells permits targeted delivery of interferon-beta and restricts tumor growth in a murine model of disseminated neuroblastoma. J Pediatr Surg. 2007; 42: 48-53.

[30] Kim S. K, Kim S. U, Park I. H, Bang J. H, Aboody K. S, Wang K. C, et al. Human neural stem cells target experimental intracranial medulloblastoma and deliver a therapeutic gene leading to tumor regression. Clin Cancer Res. 2006; 12: 5550-5556.

[31] Shimato S, Natsume A, Takeuchi H, Wakabayashi T, Fujii M, Ito M, et al. Human neural stem cells target and deliver therapeutic gene to experimental leptomeningeal medulloblastoma. Gene Ther. 2007; 14: 1132-1142.

[32] Han X, Yu L, Ren J, Wang M, Liu Z, Hu X, et al. Efficient and Fast Differentiation of Human Neural Stem Cells from Human Embryonic Stem Cells for Cell Therapy. Stem Cells Int. 2017; 9405204.

[33] Reimand J, Kull M, Peterson H, Hansen J, Vilo J. g:Profiler--a web-based toolset for functional profiling of gene lists from large-scale experiments. Nucleic acids research. 2007; 35: W193-200.

[34] Yamamuro S, Sano E, Okamoto Y, Ochiai Y, Ohta T, Ogino A, et al. Antitumorigenic effect of interferon-beta by inhibition of undifferentiated glioblastoma cells. Int J Oncol. 2015; 47: 1647-1654.

[35] Castets F, Griffin W. S, Marks A, Van Eldik L. J. Transcriptional regulation of the human S100 beta gene. Brain Res Mol Brain Res. 1997; 46: 208-216.

[36] Imbalzano E, Quartuccio S, Casciaro M, Gangemi S. S100B in heart diseases. Cardiovasc Pathol. 2020; 49: 107235.

[37] Yang C. H, Murti A, Pfeffer S. R, Basu L, Kim J. G, Pfeffer L. M. IFNalpha/beta promotes cell survival by activating NF-kappa B. Proc Natl Acad Sci U S A. 2000; 97: 13631-13636.

[38] Pfeffer L. M, Kim J. G, Pfeffer S. R, Carrigan D. J, Baker D. P, Wei L, et al. Role of nuclear factor-kappaB in the antiviral action of interferon and interferon-regulated gene expression. J Biol Chem. 2004; 279: 31304-31311.

[39] Yamazoe T, Koizumi S, Yamasaki T, Amano S, Tokuyama T, Namba H. Potent tumor tropism of induced pluripotent stem cells and induced pluripotent stem cell-derived neural stem cells in the mouse intracerebral glioma model. Int J Oncol. 2015; 46: 147-152.

[40] Tang Y, Yu P, Cheng L. Current progress in the derivation and therapeutic application of neural stem cells. Cell Death Dis. 2017; 8: e3108.

[41] Sims T. L, Hamner J. B, Bush R. A, Williams R. F, Zhou J. F, Kim S. U, et al. Neural Progenitor Cell-mediated Delivery of Interferon Beta Improves Neuroblastoma Response to Cyclophosphamide. Ann Surg Oncol. 2008; 15: 3259-3267.

[42] Ito S, Natsume A, Shimato S, Ohno M, Kato T, Chansakul P, et al. Human neural stem cells transduced with IFN-beta and cytosine deaminase genes intensify bystander effect in experimental glioma. Cancer Gene Ther. 2010; 17: 299-306.

[43] Garrison J. I, Berens M. E, Shapiro J. R, Treasurywala S, FloydSmith G. Interferon-beta inhibits proliferation and progression through S phase of the cell cycle in five glioma cell lines. J Neuro-Oncol. 1996; 30: 213-223.

[44] Happold C, Roth P, Silginer M, Florea A. M, Lamszus K, Frei K, et al. Interferon-beta Induces Loss of Spherogenicity and Overcomes Therapy Resistance of Glioblastoma Stem Cells. Mol Cancer Ther. 2014; 13: 948-961.

[45] Khsheibun R, Paperna T, Volkowich A, Lejbkowicz I, Avidan N, Miller A. Gene expression profiling of the response to interferon beta in Epstein-Barr-transformed and primary B cells of patients with multiple sclerosis. PLoS One. 2014; 9: e102331.

[46] Ohtsuka T, Nakanishi H, Ikeda W, Satoh A, Momose Y, Nishioka H, et al. Nexilin: A novel actin filament-binding protein localized at cell-matrix adherens junction. Journal of Cell Biology. 1998; 143: 1227-1238.

[47] Le Rhun E, von Achenbach C, Lohmann B, Silginer M, Schneider H, Meetze K, et al. Profound, durable and MGMT-independent sensitivity of glioblastoma cells to cyclin-dependent kinase inhibition. Int J Cancer. 2019; 145: 242-253.

[48] Su Y. T, Chen R, Wang H, Song H, Zhang Q, Chen L. Y, et al. Novel Targeting of Transcription and Metabolism in Glioblastoma. Clin Cancer Res. 2018; 24: 1124-1137.

[49] Wu J, Bryla C, Mccoy A, Lisa B, Garren N, Siegel C, et al. Phase I Trial of Tg02 Plus Dose-Dense or Metronomic Temozolomide for Adults with Recurrent Anaplastic Astrocytoma and Glioblastoma. Neuro-Oncology. 2017; 19: 15-15.

Figure Legends

Fig. 1 The growth of hGCSs but not hNSCs is inhibited by IFN-β. **a** A schematic representation showing hGCSs treated with basic media containing 10 ng/mL fibroblast growth factor (FGF), and different concentrations of IFN-β: 0, 0.625, 1.25, 2.5, 5, and 11 ng/mL. **b** The sphere-like hGCSs were inhibited, and more adherent hGCSs were observed after the IFN-β treatment. **c** IFN-β treatment resulted in smaller single sphere-like cells than control cells, and the sizes of the cell spheres are concentration-dependent within a certain range of IFN-β concentrations. **d** Coverage rate of adherent hGCSs decreased significantly with 5 ng/mL and 11 ng/mL IFN-β treatments. **e** Schematic representations of hGCSs treated with high concentrations of IFN-β. **f** High-concentration IFN-β also inhibits hGCS growth. **g** The coverage rate of hGCSs decreased after treatment with 11 ng/mL, 33 ng/mL, and 100 ng/mL IFN-β. **h** Schematic representation of hNSCs treated with high-concentration IFN-β. **i** High-concentration IFN-β does not inhibit hNSC growth. **j** The coverage rate of hNSCs does not decrease following treatment with 11 ng/mL, 33 ng/mL, and 100 ng/mL IFN-β. Quantitative data measured using ImageJ. Data are presented as the mean ± SD. Student's t-test. $*p < 0.05$, $**p < 0.01$, $***p < 0.001$.

Fig. 2 IFN-β treatment resulted in decreased numbers of Ki67-, S100-β-, and Sox2-positive cells. **a** Representative images of hGCSs immunostained for Ki67, S100-β, and Sox2, with DAPI nuclear stain. Three groups, control, 11 ng/mL, and 33ng/mL IFN-β treatment groups, were collected after 6 days of treatment (scale bar, 50 μm; white frames indicate the next part of the figure). **b** Representative images from (A), at higher magnification, using the same three groups: control, 11 ng/mL, and 33 ng/mL IFN-β treatment groups. **c** Quantitative analysis of Ki67, S100-β, Sox2, and DAPI nuclear stain in hGCSs after IFN-β stimulation, as measured by ImageJ. Data are presented as the mean ± SD. Student's t-test. $*p < 0.05$, $***p < 0.001$.

Fig. 3 Merged images showing the relative expression level of S100-β and the increased size of the cell nucleus after IFN-β stimulation. **a** Representative overlapping images showing staining for Ki67/DAPI, S100-β/DAPI, Sox2/DAPI, Ki67/S100-β, and Sox2/S100-β in hGCSs. Three groups, control, 11 ng/mL, and 33ng/mL IFN-β treatment groups (yellow frames indicate enlarged areas). **b** Representative images from (a) at higher magnification. White arrows indicate S100-β expression. Enlarged area (scale bar, 50 μm). **c** Representative images of DAPI staining and a schematic diagram of the nucleus. **d** Quantitative analysis of nuclear size, as measured using ImageJ. Scale bar, 50 μm. Data are presented as the mean ± SD. Student's t-test. $***p < 0.001$.

Fig. 4 Continuous IFN-β stimulation can enhance the inhibitory effects on hGCS growth, which differs from the effects on hNSCs. **a** Flow chart indicating the continuous stimulation timeline and imaging time points. The strategy of passage → stimulation → waiting → re-passage → stimulation → time point photography was adopted. **b** Representative hGCS images after continuous stimulation, re-passage, and stimulation, day 2. Three groups: control to control, IFN-β to control, and IFN-β to IFN-β (black frames indicate enlarged areas). **c** Representative hNSC pictures after continuous stimulation, re-passage, and stimulation, day 2. Three groups: control to control, IFN-β to control, and IFN-β to IFN-β (black frames indicate the enlarged area). **d** Representative hGCS images after continuous stimulation at re-passage, day 8. **e** Schematic diagram of hGCSs and hNSCs after re-passage and stimulation, day 2. **f-g** Quantitative analysis of hGCSs, including coverage rate (F) and single-clone area (G), of the surviving clones, as measured by ImageJ. Scale bar, 50 μm. Data are presented as the mean ± SD. Student's t-test. $**p < 0.01$, $***p < 0.001$.

Fig. 5 Transcriptome changes in hGCSs after IFN-β treatment. **a** Gene clustering from control (Con-1 and Con-2) and IFN-β treatment (IFN-1 and IFN-2) samples for the hGCSs/hNSCs RNA sequencing results. **b** Identification of significantly upregulated and downregulated genes as $hGCS^{+}$ (1,707 genes), $hGCS^{-}$ (1,338 genes), $hNSC^{+}$ (1,553 genes), and $hNSC^{-}$ (1,169 genes). **c** The Venn diagram shows the overlap among the 4 gene lists identified in (B) to identify $hGCS^{-}hNSC^{NA}$ (995 genes) and $hGCS^{+}hNSC^{NA}$ (969 genes) lists. **d** Biological process (BP) items in the Gene Ontology analysis of the $hGCS^{+}hNSC^{NA}$ gene list. **e** KEGG analysis of the $hGCS^{-}hNSC^{NA}$ gene list. **f** Expression patterns of immune response and cell adherent genes in hGCSs and hNSCs. **g** Expression patterns of cell cycle genes in hGCSs and hNSCs.

Fig. 6 IFN-β reduced cell proliferation in hGCSs. The ability to form spheres was inhibited by IFN-β. The cell and nuclear sizes of hGCSs increased after IFN-β treatment. On a gene level, significant upregulation was observed among immune response and cell adherence-related genes. Cell cycle and ribosome-related genes decreased.

Figures

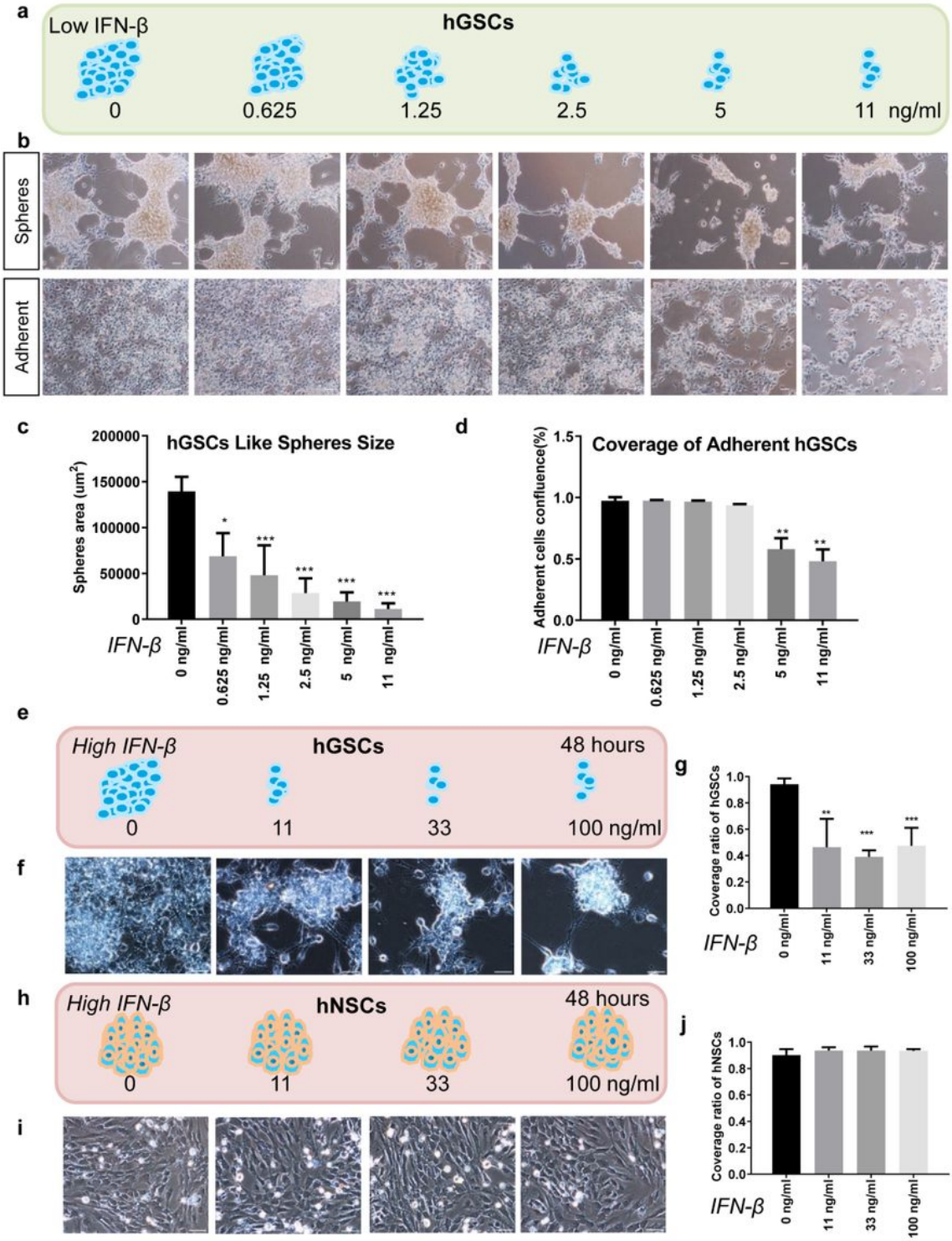

Figure 1

The growth of hGCSs but not hNSCs is inhibited by IFN-β. a A schematic representation showing hGCSs treated with basic media containing 10 ng/mL fibroblast growth factor (FGF), and different concentrations of IFN-β: 0, 0.625, 1.25, 2.5, 5, and 11 ng/mL. b The sphere-like hGCSs were inhibited, and

more adherent hGCSs were observed after the IFN-β treatment. c IFN-β treatment resulted in smaller single sphere-like cells than control cells, and the sizes of the cell spheres are concentration-dependent within a certain range of IFN-β concentrations. d Coverage rate of adherent hGCSs decreased significantly with 5 ng/mL and 11 ng/mL IFN-β treatments. e Schematic representations of hGCSs treated with high concentrations of IFN-β. f High-concentration IFN-β also inhibits hGCS growth. g The coverage rate of hGCSs decreased after treatment with 11 ng/mL, 33 ng/mL, and 100 ng/mL IFN-β. h Schematic representation of hNSCs treated with high-concentration IFN-β. i High-concentration IFN-β does not inhibit hNSC growth. j The coverage rate of hNSCs does not decrease following treatment with 11 ng/mL, 33 ng/mL, and 100 ng/mL IFN-β. Quantitative data measured using ImageJ. Data are presented as the mean ± SD. Student's t-test. *p < 0.05, **p < 0.01, ***p < 0.001.

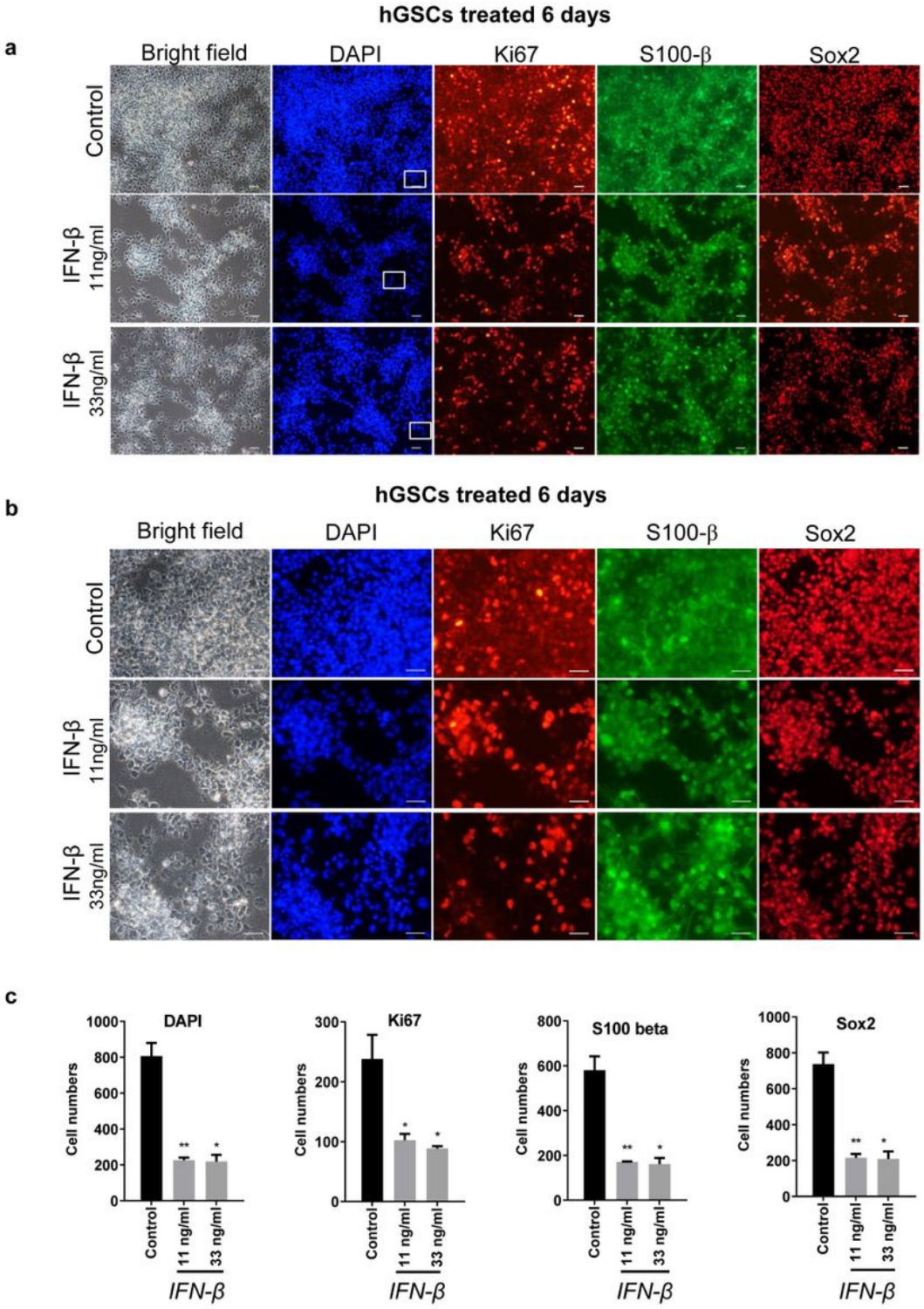

Figure 2

IFN-β treatment resulted in decreased numbers of Ki67-, S100-β-, and Sox2-positive cells. a Representative images of hGCSs immunostained for Ki67, S100-β, and Sox2, with DAPI nuclear stain. Three groups, control, 11 ng/mL, and 33ng/mL IFN-β treatment groups, were collected after 6 days of treatment (scale bar, 50 μm; white frames indicate the next part of the figure). b Representative images from (A), at higher magnification, using the same three groups: control, 11 ng/mL, and 33 ng/mL IFN-β treatment groups. c

Quantitative analysis of Ki67, S100-β, Sox2, and DAPI nuclear stain in hGCSs after IFN-β stimulation, as measured by ImageJ. Data are presented as the mean ± SD. Student's t-test. p < 0.05, p < 0.001.

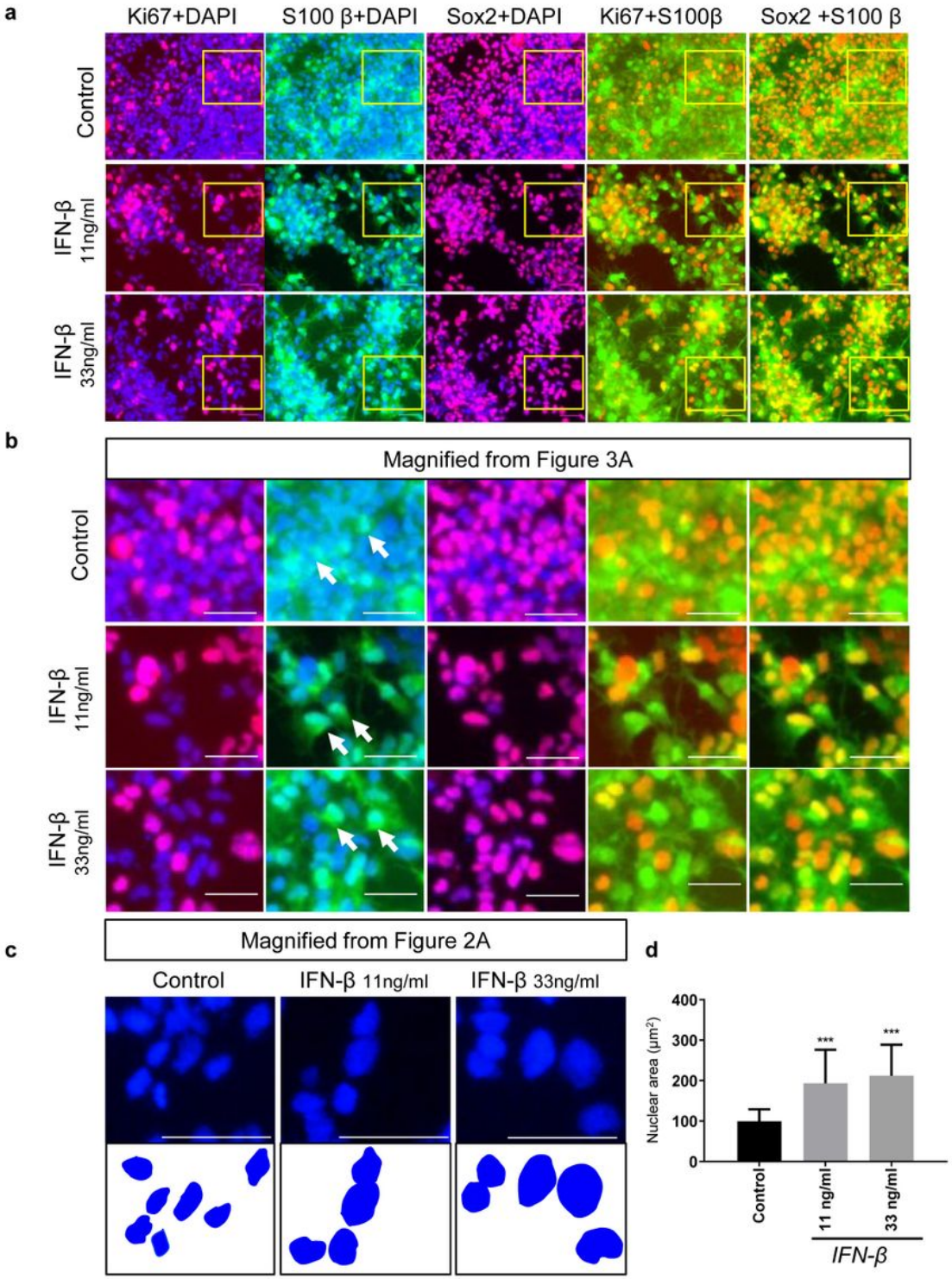

Figure 3

Merged images showing the relative expression level of S100-β and the increased size of the cell nucleus after IFN-β stimulation. a Representative overlapping images showing staining for Ki67/DAPI, S100-β/DAPI, Sox2/DAPI, Ki67/S100-β, and Sox2/S100-β in hGCSs. Three groups, control, 11 ng/mL, and

33ng/mL IFN-β treatment groups (yellow frames indicate enlarged areas). b Representative images from (a) at higher magnification. White arrows indicate S100-β expression. Enlarged area (scale bar, 50 μm). c Representative images of DAPI staining and a schematic diagram of the nucleus. d Quantitative analysis of nuclear size, as measured using ImageJ. Scale bar, 50 μm. Data are presented as the mean ± SD. Student's t-test. ***p < 0.001.

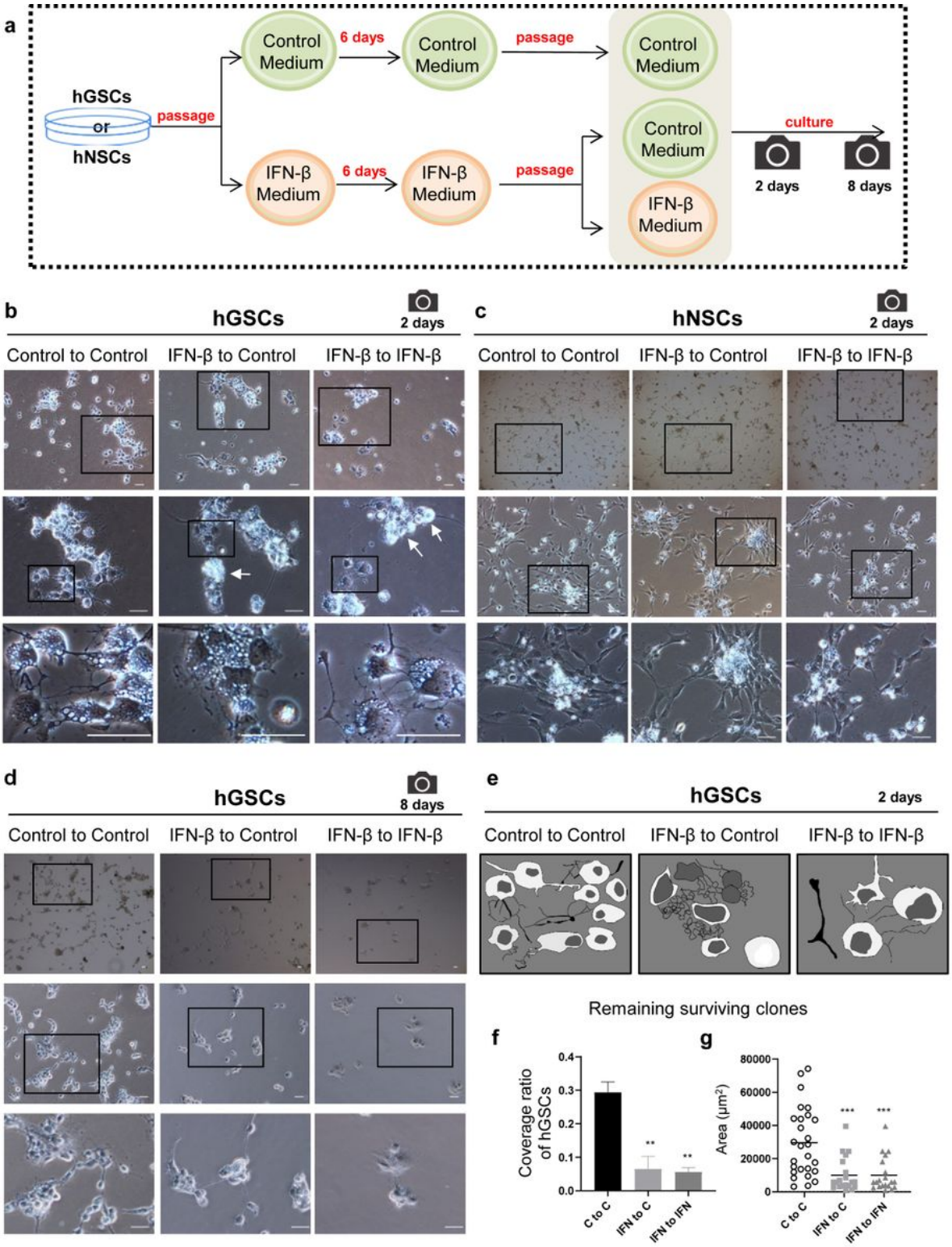

Figure 4

Continuous IFN-β stimulation can enhance the inhibitory effects on hGCS growth, which differs from the effects on hNSCs. a Flow chart indicating the continuous stimulation timeline and imaging time points. The strategy of passage → stimulation → waiting → re-passage → stimulation → time point photography was adopted. b Representative hGCS images after continuous stimulation, re-passage, and stimulation, day 2. Three groups: control to control, IFN-β to control, and IFN-β to IFN-β (black frames indicate enlarged areas). c Representative hNSC pictures after continuous stimulation, re-passage, and stimulation, day 2. Three groups: control to control, IFN-β to control, and IFN-β to IFN-β (black frames indicate the enlarged area). d Representative hGCS images after continuous stimulation at re-passage, day 8. e Schematic diagram of hGCSs and hNSCs after re-passage and stimulation, day 2. f-g Quantitative analysis of hGCSs, including coverage rate (F) and single-clone area (G), of the surviving clones, as measured by ImageJ. Scale bar, 50 μm. Data are presented as the mean ± SD. Student's t-test. $^{**}p < 0.01$, $^{***}p < 0.001$.

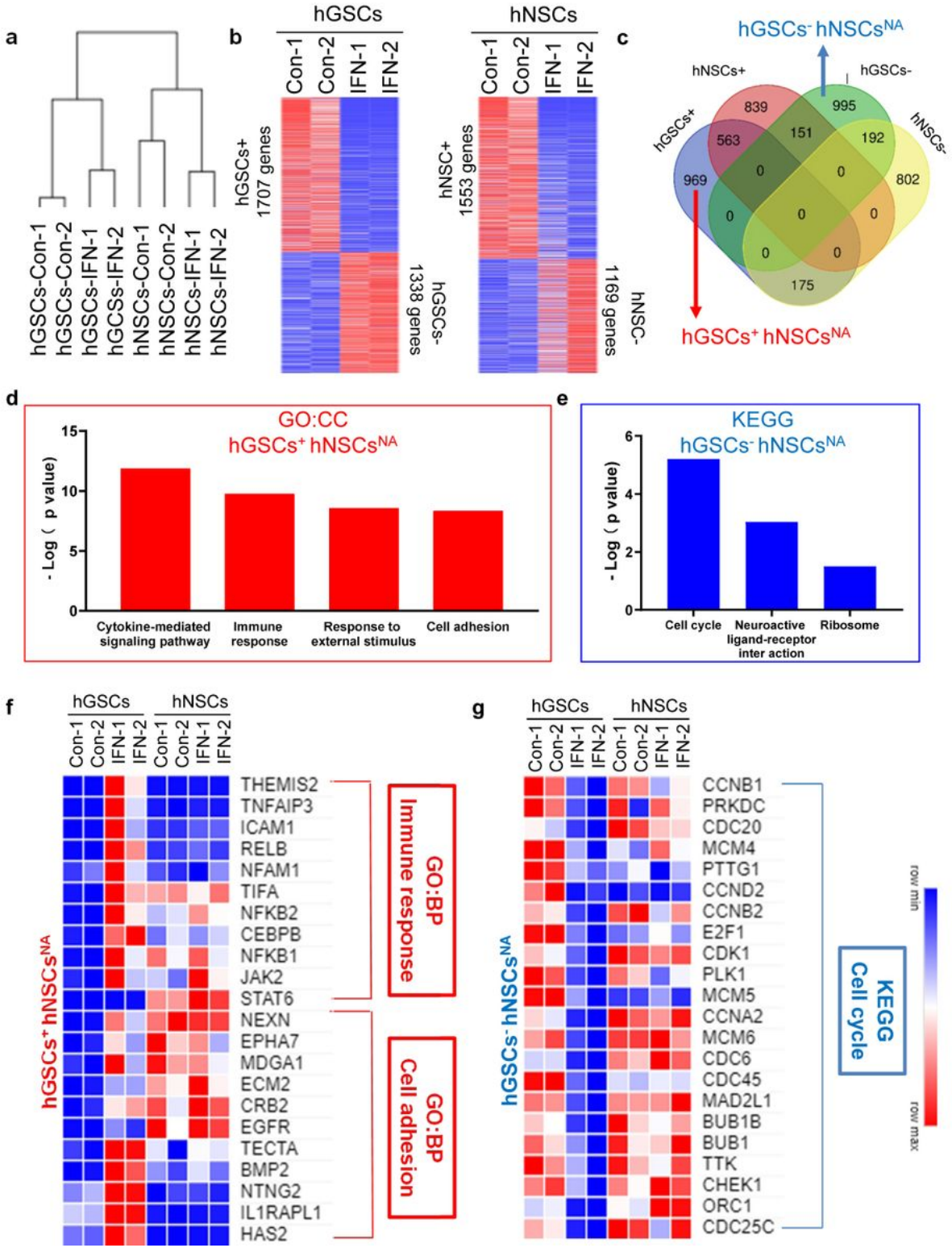

Figure 5

Transcriptome changes in hGCSs after IFN-β treatment. a Gene clustering from control (Con-1 and Con-2) and IFN-β treatment (IFN-1 and IFN-2) samples for the hGCSs/hNSCs RNA sequencing results. b Identification of significantly upregulated and downregulated genes as hGCS+ (1,707 genes), hGCS− (1,338 genes), hNSC+ (1,553 genes), and hNSC− (1,169 genes). c The Venn diagram shows the overlap among the 4 gene lists identified in (B) to identify hGCS−hNSCNA (995 genes) and hGCS+hNSCNA (969

genes) lists. d Biological process (BP) items in the Gene Ontology analysis of the hGCS+hNSCNA gene list. e KEGG analysis of the hGCS−hNSCNA gene list. f Expression patterns of immune response and cell adherent genes in hGCSs and hNSCs. g Expression patterns of cell cycle genes in hGCSs and hNSCs.

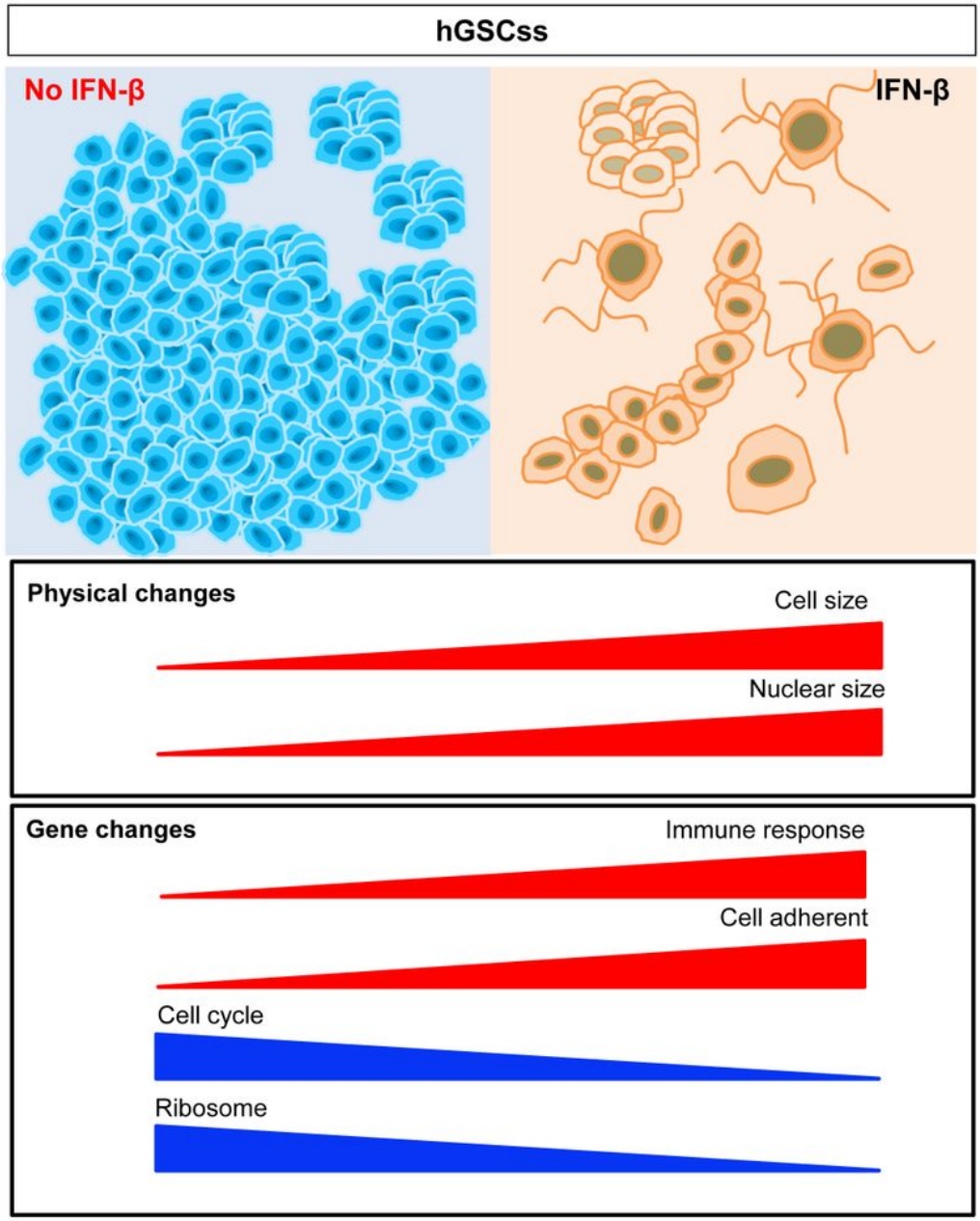

Figure 6

IFN-β reduced cell proliferation in hGCSs. The ability to form spheres was inhibited by IFN-β. The cell and nuclear sizes of hGCSs increased after IFN-β treatment. On a gene level, significant upregulation was

observed among immune response and cell adherence-related genes. Cell cycle and ribosome-related genes decreased.